AXISYMMETRIC STAGNATION – POINT FLOW AND HEAT TRANSFER OBLIQUELY IMPINGING ON A ROTATING CIRCULAR CYLINDER

A. B. Rahimi* and V. Mossavinik

Department of Mechanical Engineering, Faculty of Engineering
Ferdowsi University of Mashhad, Mashhad, Iran, P. O. Box 91775-1111
rahimiab@yahoo.com

*Corresponding Author

(**Received: July 15, 2006 - Accepted in Revised Form: January 18, 2007)**

Abstract Laminar stagnation flow, axi-symmetrically yet obliquely impinging on a rotating circular cylinder, as well as its heat transfer is formulated as an exact solution of the Navier-Stokes equations. Rotational velocity of the cylinder is time - dependent while the surface transpiration is uniform and steady. The impinging stream is composed of a rotational axial flow superposed onto irrotational radial stagnation flow normal to the cylinder with strength Γ. The relative importance of these two flows is measured by a parameter γ. The governing parameters are the stagnation - flow Reynolds number $\mathrm{Re} = \Gamma a^2 / 2\upsilon$ and the dimensionless transpiration $S = U_0 / \Gamma a$, where a is cylinder radius, ν is kinematic viscosity of the fluid and U_0 is the transpiration rate. An exact solution is obtained by reducing the Navier-Stokes equations to a system of differential equations governed by Reynolds number and the dimensionless wall transpiration rate. Dimensionless shear stresses corresponding to all the cases increase with the increase of Reynolds number and suction rate. Heat transfer is independent of cylinder rotation and its coefficient increases with the increasing suction rate, Reynolds number and Prandtl number.

Keywords Oblique Stagnation Flow, Axisymmetric, Time - Dependent Rotation, Time - Dependent Heat Transfer, Transpiration, Exact Solution

چکیده در این مساله جریان سکون متقارن مایل برخورد کننده روی یک استوانه در حال چرخش همراه با انتقال حرارت به صورت حل دقیق معادلات ناویر– استوکس فرموله می‌شود. سرعت چرخشی استوانه تابع زمان می‌باشد، ولی دمش و مکش سطحی پایدار است. جریان برخورد کننده به استوانه، ترکیبی از یک جریان محوری برهمنهش یافته با یک جریان شعاعی عمود بر این استوانه می‌باشد. حل دقیق با تبدیل معادلات ناویر – استوکس به یک سیستم معادلات دیفرانسیل با پارامترهای عدد رینولدز و نرخ دمش و کرنش بدون بعد در دیواره به دست می‌آید. تنش برشی بدون بعد مربوطه برای تمام موارد با افزایش عدد رینولدز افزایش می‌یابد. انتقال حرارت از چرخش سیلندر مستقل بوده و ضریب انتقال حرارت با افزایش نرخ مکش، عدد رینولدز و عدد پرانتل افزایش می‌یابد.

1. INTRODUCTION

An exact solution for viscous axisymmetric flow stagnation obliquely on a rotating circular cylinder as well as its heat transfer is presented here. A schematic of this flow is given in Figure 1. This study, which builds on the work of Wang [1], provides the three - dimensinal counterpart to oblique planar stagnation flow, first formulated and solved by Stuart [2]. This problem was independently reconsidered by Tamada [3] and again by Dorrepaal [4], each presenting additional results concerning the position and angle of the attaching streamline. Liu [5] and Tilley and Weidman [6] studied response of one fluid in the lower - half plane driven by an oblique stagnation flow of a second fluid in the upper - half palne. Wang was the first to investigate the stagnation flow normally directed to the surface of a circular cylinder and since then a number of variations

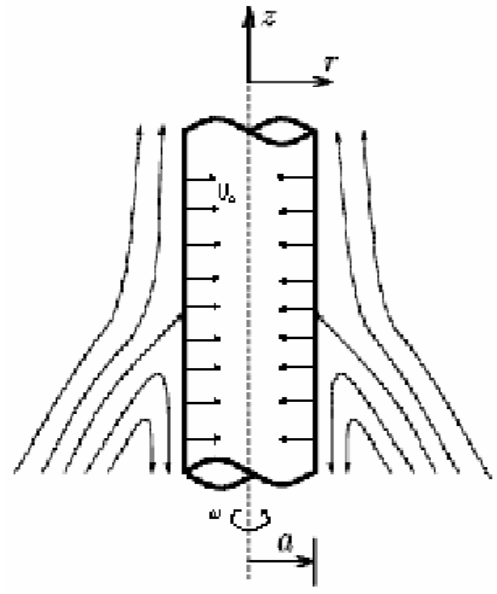

Figure 1. Schematic diagram of a rotating cylinder under oblique stagnation flow in the fixed cylindrical coordinate system (r,φ,z).

that take into account unsteady flow effects, cylinder translation and rotation and wall transpiration have appeared in the literature; see, for example, Gorla [7-9], Cunning et al. [10], Rahimi [11] and Saleh and Rahimi [12]. As pointed out by Peregrine [13], the results of the flow studied here may help to better understand the local behavior of certain viscous axisymmetric splash patterns. Also, taking into acccount the heat transfer, these axisymmetric stagnation flows may be relevant to the cooling of extruded tubes and rods using radially - inward directed fan or conical liquid jets. In the two - dimensional counterpart to the present investigation, Stuart, Tamada and Dorrepaal each realize that an outer planar oblique stagnation flow could be constructed by superposing a tangential flow of uniform shear onto planar irrotational stagnation - point flow. It is then relatively straightforward to derive the equations governing the viscous problem, comprised of a linear equation for the cross flow coupled to the nonlinear Hiemenz [14] equation governing the normal planar stagnation - point flow of a viscous fluid. Following this strategy, an outer oblique radial stagnation flow impinging on a cylinder is constructed by superposition of an appropriate axial shear flow onto inviscid radial stagnation flow impinging normal to a cylinder, Weidman and putkaradeze [15].

The effects of cylinder rotation with time - dependent angular velocity and time - dependent heat transfer along with transpiration have not yet been investigated. This study generalizes the problem of stagnation - point flow and heat transfer of a fluid obliquely impinging on a rotating cylinder. In the present analysis, the unsteady viscous flow and heat transfer in the vicinity of an axisymmetric stagnation point of an infinite rotating cylinder with uniform transpiration is considered when the angular velocity varies arbitrarily with time. An exact solution of the Navier - Stokes equations and the energy equation is obtained. The general self - similar solution is obtained when the angular velocity of the cylinder and its surface temperature or heat flux vary in a prescribed manner. The cylinder may perform different types of motion: it may rotate with constant speed (i.e., steady state cooling processes in industry, etc.), with exponentially increasing/decreasing angular velocity (i.e., start up and stopping stages of centrifugal processes in industry, etc.), with harmonically varying rotation speed, or with accelerating/decelerating oscillatory angular speed (sinusoidal blenders in industry, etc.). The cylinder surface temperature and its surface heat flux may have the same behavior as the cylinder motion. For different forms of azimuthal component of velocity, sample distribution of shear stresses and temperature fields are presented for certain values of Reynolds numbers and different values of Prandtl numbers, Pr and selected values of uniform suction and blowing rates. Particular cases of these results are compared with existing results of Ref. [15]. For completeness, some semi - similar solutions of the Navier - Stokes equations are obtained and results, for example, of cylinder rotation in the form of a step - function is presented for selected values of flow parameters. The stream surfaces are shown and the deflection of the stagnation circle from its assumed location is calculated.

2. PROBLEM FORMULATION

We consider the laminar unsteady incompressible flow and heat transfer of a viscous fluid in the neighborhood of an axisymmetric stagnation - point of an infinite rotating circular cylinder with uniform normal transpiration U_0 at its surface, where $U_0 > 0$ corresponds to suction into the cylinder. The flow configuration is shown in Figure 1 in cylindrical coordinates (r,φ,z) with corresponding velocity components (u,v,w). The cylinder rotates with time - dependent angular velocity ω and the wall temperature or the wall heat flux is also a function of time. The external impinging stream is composed of a rotational axial flow surposed onto irrotational radial stagnation flow normal to the cylinder with strenght Γ. The relative importance of these two flows is measured by a parameter γ. The cylinder radius is *a*, centered at r = 0. The location of the stagnation - circle of the inviscid outer flow is at z = 0. The unsteady Navier - Stokes and energy equations in cylindrical polar coordinates governing the axisymmetric flow and heat transfer are given by [1,7,8]:

Mass:

$$\frac{\partial}{\partial r}(ru)+r\frac{\partial w}{\partial z}=0 \tag{1}$$

Momentum:

$$\frac{\partial u}{\partial t}+u\frac{\partial u}{\partial r}-\frac{v^2}{r}+w\frac{\partial u}{\partial z}= -\frac{1}{\rho}\frac{\partial p}{\partial r}+\upsilon\left(\frac{\partial^2 u}{\partial r^2}+\frac{1}{r}\frac{\partial u}{\partial r}-\frac{u}{r^2}+\frac{\partial^2 u}{\partial z^2}\right) \tag{2}$$

$$\frac{\partial v}{\partial t}+u\frac{\partial v}{\partial r}+\frac{uv}{r}+w\frac{\partial v}{\partial z}= \upsilon\left(\frac{\partial^2 v}{\partial r^2}+\frac{1}{r}\frac{\partial v}{\partial r}-\frac{v}{r^2}+\frac{\partial^2 v}{\partial z^2}\right) \tag{3}$$

$$\frac{\partial w}{\partial t}+u\frac{\partial w}{\partial r}+w\frac{\partial w}{\partial z}= -\frac{1}{\rho}\frac{\partial p}{\partial z}+\upsilon\left(\frac{\partial^2 w}{\partial r^2}+\frac{1}{r}\frac{\partial w}{\partial r}+\frac{\partial^2 w}{\partial z^2}\right) \tag{4}$$

Energy:

$$\frac{\partial T}{\partial t}+u\frac{\partial T}{\partial r}+w\frac{\partial T}{\partial z}=\bar{\alpha}\left[\frac{1}{r}\frac{\partial}{\partial r}\left(r\frac{\partial T}{\partial r}\right)+\frac{\partial^2 T}{\partial z^2}\right] \tag{5}$$

where p,ρ,υ and $\bar{\alpha}$ are the fluid pressure, density, kinematic viscosity and thermal diffusivity. The boundary conditions for the velocity field are:

$$r=a:\quad u=-U_0(t),\qquad v=a.\omega(t),\quad w=0 \tag{6}$$

$$r\to\infty:\frac{\partial u}{\partial r}=-\Gamma,\qquad \lim_{r\to\infty} r\,v=0,\quad w=2\Gamma z+\frac{\gamma}{2}(r^2/a^2-1) \tag{7}$$

Here, relations 6 are transpiration and no-slip boundary conditions on the cylinder wall, where $U_0(t)$ is the transpiration rate and ω(t) is the angular velocity of the cylinder. Relations 7 show that the viscous flow solution approaches, in a manner analogous to the Hiemenz flow, the potential stagnation field as r→∞, Ref. [10]. This is imposing the conditions of zero circulation at infinity on the swirl velocity of the stagnation flow.

For the temperature field we have:

$$r=a:\quad i)T=T_w(t)\quad \text{for defined wall temperature}$$

$$ii)\frac{\partial T}{\partial r}=-\frac{q_w(t)}{k}\quad \text{for defined wall heat flux}$$

$$r\to\infty:\quad T\to T_\infty \tag{8}$$

where K is the thermal conductivity of the fluid and $T_w(t)$ and $q_w(t)$ are temperature and heat flux at the wall cylinder, respectively.

A reduction of the Navier - Stokes equations is obtained by applying the following transformations:

$$u=-\Gamma\frac{a}{\sqrt{\eta}}f(\eta,\tau),\quad v=\frac{a}{\sqrt{\eta}}G(\eta,\tau),\quad w=2\Gamma f'(\eta,\tau)z+\frac{\gamma}{2}g'(\eta),\ p=\rho\Gamma a^2 P \tag{9}$$

where $\tau = 2\Gamma t$ and $\eta = (r/a)^2$ are dimensionless time and radial variables and prime denotes differentiation with respect to η. Transformations 9 satisfy 1 automatically and their insertion into Equation 2 yields a differential equation in terms of $f(\eta,\tau)$ as following:

$$\eta f''' + f'' + Re[1-(f')^2 + ff'' - \frac{\partial f'}{\partial \tau}] = 0 \qquad (10)$$

where $Re = \Gamma a^2/2\upsilon$ is the Reynolds number. From conditions 6 and 7, the boundary conditions for 10 are:

$$\eta = 1: \quad f = S(\tau),\ f' = 0 \qquad \eta \to \infty : f' = 1$$

in which $S(\tau) = \frac{U_0(\tau)}{\Gamma a}$ is the dimensionless wall - transpiration rate.

For the brevity, only results for $S(\tau)$ = constant are shown in this paper. For $S(\tau)$ = constant, none of the boundary conditions of Equation 10 are function of time and assuming steady - state initial conditions for this equation, we have:

$$\tau = 0 \to \frac{\partial f'}{\partial \tau} = 0$$

Therefore in this case $f(\eta,\tau) = f(\eta)$ and Equation 10 is reduced to the following form:

$$\eta f''' + f'' + Re[1-(f')^2 + f f''] = 0 \qquad (11)$$

Insertion of transformations 9 into 3 and 4 yields two differential equations in terms of $f(\eta)$, $g(\eta)$ and $G(\eta,\tau)$ and an expression for the pressure:

$$\eta g''' + g'' + Re\,(f g'' - f' g') = 0 \qquad (12)$$

$$\eta G'' + Re\,[f G' - \frac{\partial G}{\partial \tau}] = 0 \qquad (13)$$

$$P - P_o = -[\frac{f^2}{2\eta} + \frac{1}{Re} f' + 2(\frac{z}{a})^2 - \frac{1}{2\Gamma^2}\int_1^\eta \frac{G^2(\xi)}{\xi^2} d\xi] \qquad (14)$$

From conditions 6 and 7, the boundary conditions for 12 and 13 are as following:

$$\eta = 1: \ g = 0,\ g' = 0,\ G = \omega(\tau) \qquad (15)$$

$$\eta \to \infty: \ g'' = 1,\ G = 0 \qquad (16)$$

To transform the energy equation into a non - dimensional form for the case of defined wall temperature, we introduce

$$\Theta = \frac{T(\eta,\tau) - T_\infty}{T_W(\tau) - T_\infty} \qquad (17)$$

Making use of 9 and 17, the energy equation may be written as:

$$\eta \Theta'' + \Theta' + Re\,Pr(f\,\Theta' - \frac{\partial \Theta}{\partial \tau} - \frac{dT_W/d\tau}{T_W - T_\infty}\Theta) = 0 \qquad (18)$$

with the boundary conditions as:

$$\Theta(1,\tau) = 1, \quad \Theta(\infty,\tau) = 0 \qquad (19)$$

For the case of defined wall heat flux, we introduce

$$\theta = \frac{T(\eta,\tau) - T_\infty}{a\, q_W(\tau)/2k} \qquad (20)$$

Now making use of 9 and 20, the energy equation can be written as:

$$\eta \Theta'' + \Theta' + Re\,Pr\,(f\Theta' - \frac{\partial \Theta}{\partial \tau} - \frac{dq_W/d\tau}{q_W}\Theta) = 0 \qquad (21)$$

with the boundary conditions as:

$$\Theta'(1,\tau) = -1, \quad \Theta(\infty,\tau) = 0 \qquad (22)$$

Here, Equations 11-13 and 18 or 21 are for different forms of $s(\tau)$, $\omega(\tau)$, $T_w(\tau)$ or $q_w(\tau)$ functions and have been solved numerically with Re and Pr as parameters.

In what follows, first the self - similar equations and the exact solutions of some particular $\omega(\tau)$, $T_w(\tau)$ or $q_w(\tau)$ functions are presented. The semi - similar solutions can be obtained for given values of $\omega(\tau)$ computationally.

3. SELF - SIMILAR EQUATIONS

Equations 13 and 18 or 21 can be reduced to ordinary differential equations if we assume that the function $G(\eta,\tau)$ in 13 and $\Theta(\eta,\tau)$ in 18 or 21 are separable as:

$$G(\eta,\tau) = m(\eta).(\tau)$$
$$\Theta(\eta,\tau) = \theta(\eta).Q(\tau) \quad (23)$$

Substituting these separation of variables into 13 and 18 or 21, correspondingly gives:

$$\eta\frac{m''}{m} + Re\, f\frac{m'}{m} = Re\frac{d\varphi(\tau)/d\tau}{\varphi(\tau)} \quad (24)$$

$$\eta\frac{\theta''}{\theta} + \frac{\theta'}{\theta} + Re\ Pr(f\theta'/\theta) = Re\,Pr\left(\frac{dQ/d\tau}{Q} + \frac{dT_w/d\tau}{T_w - T_\infty}\right) \quad (25)$$

or for defined wall heat flux:

$$\eta\frac{\theta''}{\theta} + \frac{\theta'}{\theta} + Re\ Pr\ (f\theta'/\theta\theta = Re\,Pr\left(\frac{dQ/d\tau}{Q} + \frac{dq_w/d\tau}{q_w}\right) \quad (26)$$

where again prime denotes differentiation with respect to η. Solutions to the differential equations in 24 and 25 or 26 with τ as an independent variable are as the following:

$$\phi(\tau) = b\ Exp[(\alpha + i\beta)\tau] \quad (27)$$

$$Q(\tau) = \frac{c\ Exp[(\xi + i\delta)\tau]}{T_w(\tau) - T_\infty} \quad (28)$$

or for defined wall heat flux:

$$Q(\tau) = \frac{c\ Exp[(\xi + i\delta)\tau]}{q_w(\tau)} \quad (29)$$

Here, $i = \sqrt{-1}$ and b, α and β and also c, ξ and δ are constants. The boundary conditions are:

$G(1,\tau) = \omega(\tau) = \phi(\tau)m(1) \rightarrow \phi(\tau) = \omega(\tau)$ and $m(1) = 1$, gives:

$$\omega(\tau) = b\ Exp[(\alpha + i\beta)\tau \quad (30)$$

$$G(\infty,\tau) = 0 = \phi(\tau)\ m(\infty) \rightarrow m(\infty) = 0 \quad (31)$$

For the above - defined wall temperature and wall heat flux, respectively, one obtains:

$$\Theta(1,\tau) = 1 = \theta(1)Q(\tau) \rightarrow \theta(1) = 1, Q(\tau) = 1 \rightarrow T_w(\tau) - T_\infty = c\ Exp[(\xi + i\delta)\tau]$$

$$\Theta'(1,\tau) = -1 = \theta'(1)\ Q(\tau) \rightarrow \theta'(1) = -1, Q(\tau) = 1 \rightarrow q_w(\tau) = c\ Exp[(\xi + i\delta)\tau] \quad (32)$$

$$\Theta(\infty,\tau) = 0 = \theta(\infty)\ Q(\tau) \rightarrow \theta(\infty) = 0 \quad (33)$$

Substituting the solutions 27, 28, or 29 into the differential equations in 24 and 25 or 26 with η as independent variable results in:

$$\eta m'' + Re[fm' - \alpha m - i\beta m] = 0 \quad (34)$$

$$\eta\theta'' + \theta' + Re\ Pr\ (f\theta' - \xi\theta - i\delta\theta) = 0 \quad (35)$$

Note that, in 30 b = 0 corresponds to the case of non - rotating cylinder, as of Weidman et al. [15]. If b = 0 and $\gamma = 0$, 30 corresponds to the case of non - rotating cylinder with normal stagnation flow, as of Wang [1]. $b \neq 0$, $\alpha = \beta = 0$ and $\gamma = 0$, 30 gives the case of a uniformly rotating cylinder with constant angular velocity, Cunning et al. [10]. $b \neq 0$, $\alpha \neq 0$ and $\beta = 0$, corresponds to the case of rotating cylinder with an exponential angular velocity. $b \neq 0$, $\beta \neq 0$ and $\alpha = 0$, corresponds to the case of pure harmonic rotation of the cylinder. The case of non - zero b, α and β is the most general case which is considered in this paper. If b = 0 and $c \neq 0$, $\gamma = \xi = \delta = 0$, Equations 32 corresponds to the result of Gorla [8] which is for a non - rotating cylinder. Other combinations of values of c, ξ and δ in Equations 32 give the different time - dependent wall temperature and wall heat flux functions.

To obtain solutions of Equations 34 and 35, it is assumed that the functions $m(\eta)$ and $\theta(\eta)$ are complex functions as:

$$m(\eta) = m_1(\eta) + im_2(\eta) \quad (36)$$

$$\theta(\eta) = \theta_1(\eta) + i\theta_2(\eta) \quad (37)$$

Substituting 36 and 37 into 34 and 35, the following coupled systems of differential equations are obtained:

$$\begin{cases} \eta m_1'' + \mathrm{Re}\,(f m_1' - \alpha m_1 + \beta m_2) = 0 \\ \eta m_2'' + \mathrm{Re}\,(f m_2' - \alpha m_2 - \beta m_1) = 0 \end{cases} \quad (38)$$

$$\begin{cases} \eta \theta_1'' + \theta_1' + \mathrm{Re\,Pr}\,(f\theta_1' - \xi\theta_1 + \delta\theta_2) = 0 \\ \eta \theta_2'' + \theta_2' + \mathrm{Re\,Pr}\,(f\theta_2' - \xi\theta_2 - \delta\theta_1) = 0 \end{cases} \quad (39)$$

Considering the boundary conditions 6, 7, the boundary conditions for functions f, m and θ become:

$$\eta = 1: \quad f = 0, \quad f' = 0, \quad m = 1, \quad \theta = 1 (\text{or } \theta' = -1) \quad (40)$$

$$\eta \to \infty: f' = 1, \quad m = 0, \quad \theta = 0 \quad (41)$$

Hence, the boundary conditions on functions m_1, m_2 and θ_1, θ_2 are:

$$\eta = 1: \quad m_1 = 1, \quad m_2 = 0, \quad \theta_1 = 1\,(\text{or } \theta_1' = -1), \quad \theta_2 = 0 \quad (42)$$

$$\eta \to \infty: m_1 = 0, \quad m_2 = 0, \quad \theta_1 = 0, \quad \theta_2 = 0 \quad (43)$$

The coupled system of Equations 38 and 39 along with boundary conditions 42 and 43 have been solved by using the fourth - order Runge - Kutta method of numerical integration along with a shooting method, Press et al. [16]. Using this method, the initial values of $m_1'(1), m_2'(1)$, θ_1' (or $\theta_1(1)$) and $\theta_2'(1)$ were guessed and the integration was repeated until convergence was obtained. The values of $m_2(\eta) = 0$ and $\theta_2(\eta) = 0$ were assumed initially and then by repeating the integration of these two systems of equations, final values of $m_1 = (\eta)$, $m_2 = (\eta)$, $\theta_1(\eta)$ and $\theta_2(\eta)$ were obtained.

The angular velocity is:

$$\omega(\tau) = b\,\mathrm{Exp}(\alpha\tau)[\cos(\beta\tau) + i\sin(\beta\tau)] \quad (44)$$

and thus, the azimuthal component of velocity from definition 9 becomes:

$$v(\eta,\tau) = \frac{a\,b}{\sqrt{\eta}}\,\mathrm{Exp}(\alpha\tau) [\{m_1(\eta)\cos(\beta\tau) - m_2(\eta)\sin(\beta\tau)\} + i\{m_1(\eta)\sin(\beta\tau) + m_2(\eta)\cos(\beta\tau)\}]. \quad (45)$$

4. SHEAR STRESSES

The shear stress at the cylinder surface is calculated from, [9]:

$$\sigma = \mu[\, r\frac{\partial}{\partial r}(\frac{v}{r})\,\hat{e}_\varphi + \frac{\partial w}{\partial r}\hat{e}_z\,] \quad (46)$$

where μ is the fluid viscosity. Using definition 9, the shear - stress at the cylinder surface for semi - similar solutions becomes

$$\sigma = 2\,\mu\,[G'(1,\tau) - \omega(\tau)]\hat{e}_\varphi + \frac{2\mu}{a}[2\Gamma z f''(1) + \frac{\gamma}{2} g''(1)] \quad (47)$$

Thus the axial and azimuthal shear stress components are proportional to $[f''(1) + g''(1)]$ and $[G'(1,\tau) - \omega(\tau)]$, respectively. Azimuthal surface shear stress for self - similar solutions is presented by the following relation:

$$\sigma_\varphi = \sigma_{\varphi_1} + i\sigma_{\varphi_2} = 2\mu b\,\mathrm{Exp}(\alpha\tau) [\{\cos(\beta\tau)(m_1'(1) - 1) - \sin(\beta\tau)m_2'(1)\} + + i\{\sin(\beta\tau)(m_1'(1) - 1) + \cos(\beta\tau)m_2'(1)\}]. \quad (48)$$

Some numerical values of real part of σ_φ will be presented later for few examples of angular velocities. Of course, it is noted that the real and imaginary parts of this quantity are actually the same but with a phase diffeference of π/2.

5. HEAT TRANSFER COEFFICIENT

The local heat transfer coefficient and rate of heat

transfer for defined wall temperature case are given by:

$$h = \frac{q_w}{T_w - T_\infty} = \frac{-k(\frac{\partial T}{\partial r})_{r=a}}{T_w - T_\infty} = -\frac{2k}{a}\Theta'(1,\tau)$$

for semi - similar case

$$h = -\frac{2k}{a}[\theta'_1(1) + i\theta'_2(1)]$$

for self - similar case

(49)

or in terms of Nusselt number:

$$Nu = \frac{ha}{2k} = Nu_r + iNu_i = -[\theta'_1(1) + i\theta'_2(1)]$$

$$q_w = -\frac{2k}{a}\Theta'(1,\tau)(T_w - T_\infty)$$

for semi - similar case

$$q_w = -\frac{2k}{a}c.$$
$$\mathrm{Exp}(\gamma\tau)[\{\theta'_1(1)\cos(\delta\tau) - \theta'_2(1)\sin(\delta\tau)\} + i\{\theta'_1(1)\sin(\delta\tau) + \theta'_2(1)\cos(\delta\tau)\}]$$

for self - similar case

(50)

and for defined wall heat flux case:

$$h = \frac{q_w}{T_w - T\infty} = \frac{2k}{a}\frac{1}{\Theta(1,\tau)}$$

for semi - similar case

$$h = \frac{2k}{a}(\frac{1}{\theta_1(1) + i\theta_2(1)})$$

for self - similar case

or in terms of Nusselt number:

$$Nu = \frac{ha}{2k} = Nu_r + iNu_i = (\frac{1}{\theta_1(1) + i\theta_2(1)})$$

(51)

$$(T_w - T_\infty) = \frac{a}{2k}\Theta(1,\tau)q_w$$

for semi - similar

$$(T_w - T_\infty) = \frac{a}{2k}c\,\mathrm{Exp}(\gamma\tau)[\{\theta_1(1)\cos(\delta\tau) - \theta_2(1)\sin(\delta\tau)\} + i\{\theta_1(1)\sin(\delta\tau) + \theta_2(1)\cos(\delta\tau)\}]$$

(52)

for self - similar case.

From 49 and 51, it is seen clearly that for self - similar cases, the local heat transfer coefficient is not a function of time contrary to the fact that wall temperature and wall heat flux are time - dependent.

6. STREAMLINES

Following Weidman and Putkaradze [15], streamline patterns are readily obtained by evaluation of the dimensionless streamfunction

$$\psi(\eta, z) = \frac{z}{2}f(\eta) + \frac{\gamma}{4}g(\eta) \qquad (53)$$

A typical streamline pattern is calculated in terms of Re and γ. From these patterns it is observed that the stagnation circle lies to the left of the origin and that the origin is the stagnation circle for the outer inviscid flow. Moreover, the slope of the viscous dividing streamline at attachment is greater than the attachment slope of the outer inviscid dividing streamline. Define $m = m_I$ as the slope of the inviscid dividing streamline at attachment and m_s as the attachment slope of the viscous dividing streamline; furthermore, define Z_s as the axial position of the viscous stagnation circle. Mathematical expressions for m_s and Z_s are readily calculated. The dividing streamsurface $\Psi = 0$ intersects the cylinder at the axial position for which the shear stress is zero. This position

determined from 47 is

$$Z_s = -\frac{\gamma}{2}\frac{g''(1)}{f''(1)} \tag{54}$$

The slope of the dividing streamline at attachment is computed from the limit:

$$m_s = \left(\frac{dr}{dz}\right)_{r\to 1} = -\lim_{\eta\to 1}\left(\frac{f'^2}{f g' - g f'}\right) \tag{55}$$

Which is indeterminate. Four successive application of L'Hopital's rule finally yield:

$$m_s = -\frac{3}{\gamma \mathrm{Re}}\frac{(f''(1))^2}{g''(1)} \tag{56}$$

In the planar problem, Dorrepaal [4] has shown that the ratio $m_s/m = 3.74851$ is independent of γ, while the independence on γ is also true here, the ratio m_s/m now depends on Re through the relation

$$m_s/m = \frac{3}{2\mathrm{Re}}\frac{(f''(1))^2}{g''(1)} \tag{57}$$

Some examples of streamline patterns are shown in the next section.

7. PRESENTATION OF RESULTS

In this section, only the real part of the solution of the self - similar Equations 34-35 and the semi - similar Equation 13 along with surface shear - stresses and heat transfer coefficient for different functions of angular velocity and prescribed values of wall temperature or wall heat flux, and selected values of suction and blowing rates are presented. Also, the real part of azimuthal component of velocity, $v(\eta,\tau)$, for self - similar case is given.

Sample profiles of the f function in terms of η are shown in Figure 2, for selected values of transpiration rate and Reynolds number. This function, for the first time, was solved by Wang [5] for the case of S = 0 and later was presented by

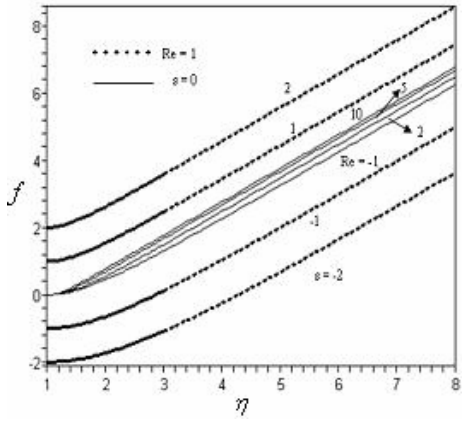

Figure 2. Sample profiles of f(η) function for selected values of suction rate and Reynolds number.

Cunning [10] for selected values of suction rate. It is evident from this figure that as Reynolds number increases the f function increases a little and approaches the inviscid solution in the limit. In this figure the dash - dot curves present the variations of f function in terms of transpiration rate in which negative S is blowing rate and positive S is the suction rate. Sample profiles of the f' and f'' functions in terms of η are depicted in Figures 3 and 4 for selected values of transpiration rate and Reynolds number. From these figures, the initial slope of the f' function $(f''(1))$ increases with increasing Reynolds number and transpiration rate and causes its limiting solution approach to one in quicker manner. From relations 9 and 47, f' presents the velocity profile in z direction and $f''(1)$ is the value of wall shear - stress in this direction. Therefore, the increase of suction rate and Reynolds number increases the wall shear - stress in z direction and on the other hand causes that the value of fluid velocity in this direction approaches its value in inviscid flow, rapidly. In fact the increase of suction rate and Reynolds number decrease the thickness of the boundary layer.

Sample profiles of the $g(\eta)$ function in terms of η are presented in Figure 5 for selected values of Reynolds number. This function is the main parameter in defining the flow stream function and thus drawing the streamlines. As it is expected, the

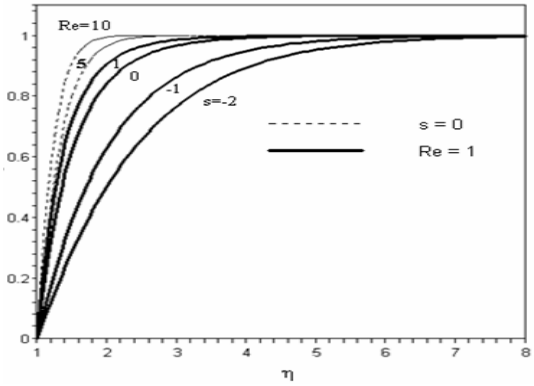

Figure 3. Sample profiles of $f'(\eta)$ function for selected values of suction rate and Reynolds number.

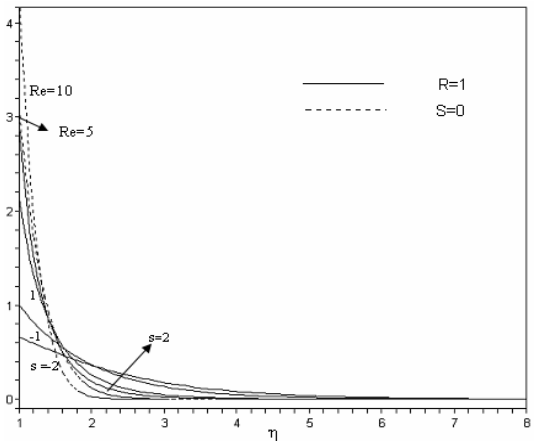

Figure 4. Sample profiles of $f''(\eta)$ function for selected values of suction rate and Reynolds number.

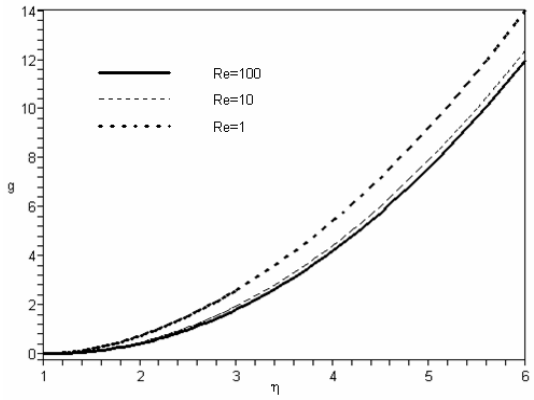

Figure 5. Sample profiles of $g(\eta)$ function for selected values of Reynolds function.

value of $g(\eta)$ is increased as Reynolds number is increasing and this causes the increase of the flow momentum. In Figure 6 the $g(\eta)$ function is shown for selected values of transpiration rate and at Re = 1. As it is seen the value of this function is increased rapidly by increasing suction rate and decreases by increasing the blowing rate. Figure 7 presents the function $g'(\eta)$ at Re = 1 and selected values of transpiration rate. This function is another main factor in determining the axial velocity in boundary layer on the cylinder and as it is seen from the figure it starts from $g'(1) = 0$ and after increasing inside the bounadry layer its behavior is linear outside this layer and $g'(\eta) \approx 0$ as $S \to -\infty$ and the axial velocity will be $w = 2\Gamma f'(\eta,\tau)z$. Sample profiles of $g''(\eta)$ are shown in Figure 8 for selected values of transpiration rates and at Re = 1. This quantity is one of the factors in determining stress tensor on the cylinder and as it is seen from this figure the value of $g''(1)$ decreases as Reynolds number increases. Also, as suction rate increases $g''(1)$ increases rapidly which is in the direction of increasing stress tensor and in the case of blowing $g''(1) \to 0$ which in the direction of decreasing stress tensor.

Sample profiles of $m(\eta)$ function for $\omega(\tau)$ in exponential form for accelerating and decelerating case at Re = 1.0 are presented in Figure 9, for selected values of transpiration rate. It is interesting to note that as α or suction rate increases, the depth of the diffusion of the fluid velocity field decreases, and it increases as α or suction rate decreases. For $\alpha < 0$, at any rate of suction and for the absolute value of α greater than a certain value, the fluid velocity in the vicinity of the cylinder cannot decrease with the same rate as the cylinder rotation velocity and therefore in this region the fluid velocity is greater than the cylinder velocity. Note, $\alpha = 0$ indicates the case of a rotating cylinder with constant angular velocity, Ref. [13].

Sample profiles of $m_1 = (\eta)$ function for $\omega(\tau)$ for accelerating and decelerating oscillatory motion and pure harmonic motion of the cylinder at Re = 1000 displyed in Figure 10 for transpiration rate of S = 0 show that like the exponential angular velocity case, the depth of the diffusion of the fluid velocity field for $\alpha > 0$ is less and for $\alpha < 0$ is more than that for the case of

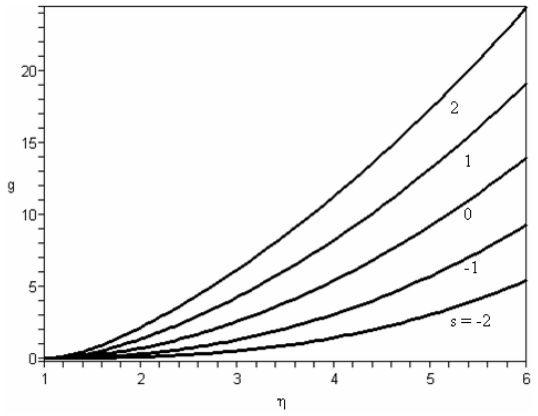

Figure 6. Sample profiles of $g(\eta)$ function for selected values of transpiration rates, at Re = 1.0.

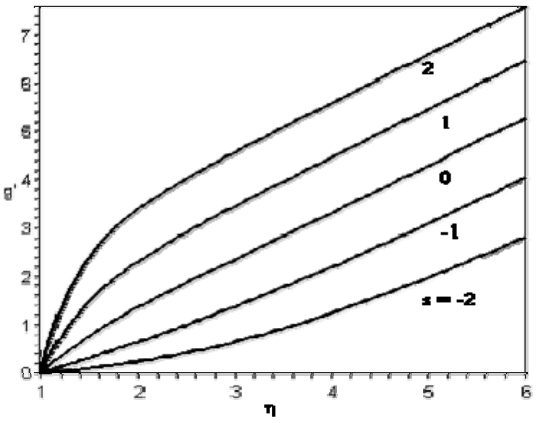

Figure 7. Sample profiles of $g'(\eta)$ function for selected values of transpiration rates, at Re = 1.0.

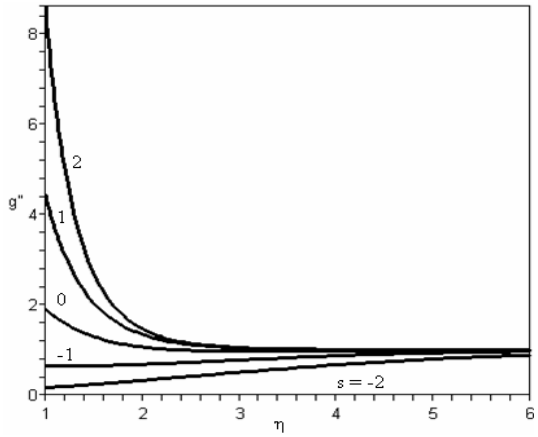

Figure 8. Sample profile of $g''(\eta)$ function for selected values of transpiration rates, at Re = 1.0.

$\alpha = 0$. Further, it is concluded that the case of $\alpha = \beta = 0$ is the same as in Ref. [14] and clearly the imaginary part of $m(\eta)$ is zero. As in the foregoing discussion, we observe that the thinning of the difussion of the velocity field with increasing values of β is evident.

Sample profiles of $m_1'(\eta)$ is shown in Figure 11 for constant rotational speed and selected values

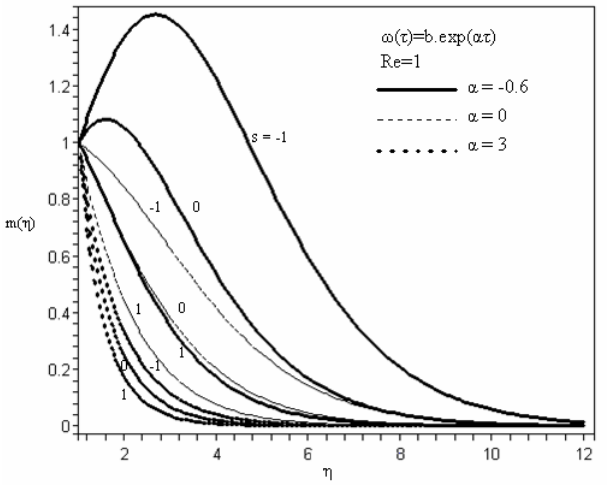

Figure 9. Sample profiles of $m(\eta)$ for cylinder with exponential angular velocity for Re = 1. and selected values of suction and α.

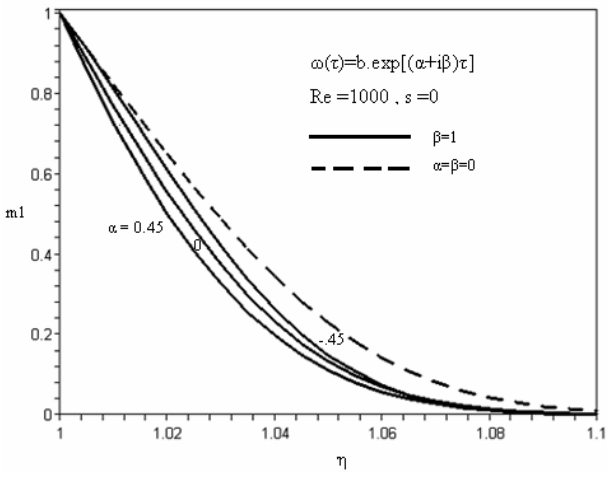

Figure 10. Sample profiles of real part of azimuthal velocity in terms of time for cylinder with harmonic rotation, for Re = 1000., s = 0.

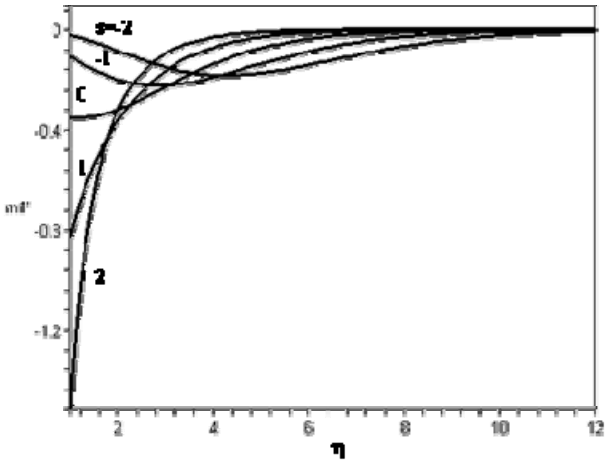

Figure 11. Sample profiles of derivative of real part of azimuthal velocity for constant rotation case for selected values of transpiration rate at Re = 1.

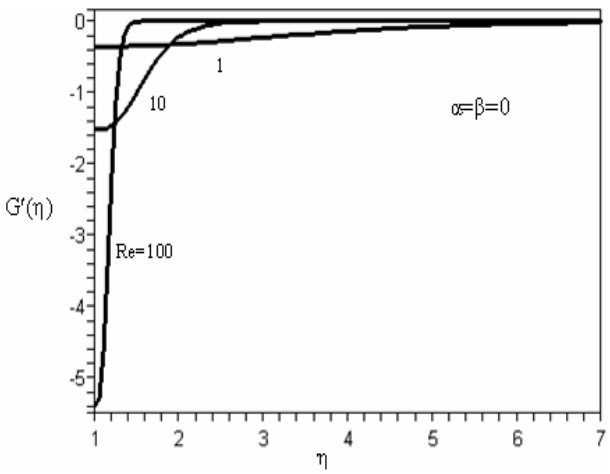

Figure 12. Sample profile of $G'(\eta)$ function for S = 0 and selected values of Reynolds number.

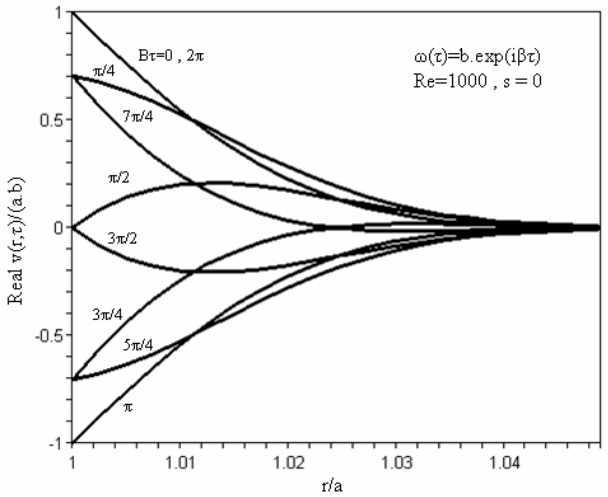

Figure 13. Azimuthal velocity in terms of time for cylinder with harmonic rotation, for Re = 1000., s = 0.

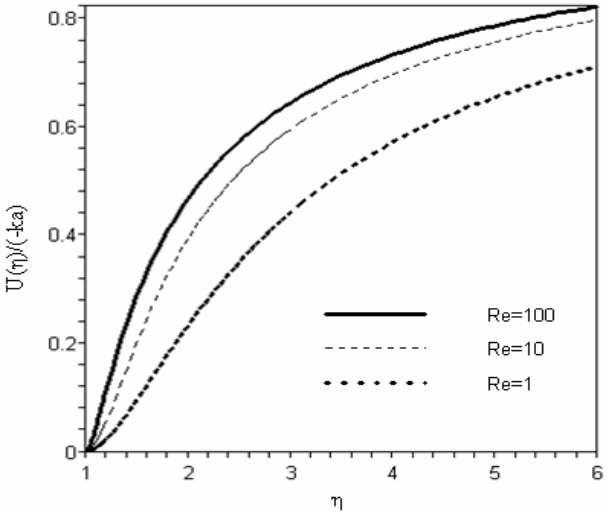

Figure 14. Sample profiles of radial velocity for S = 0 and at selected values of Reynolds numbers.

of transpiration rate at Re = 1.0. This function produces the tangential stress tensor which increases rapidly as the suction rate increases and as $S \to -\infty$, this function tends to zero.

Sample profiles of G'(η) in terms of η with no transpiration and for the case of constant rotational speed is shown in Figure 12 for selected values of Reynolds numbers. As it is seen from the figure, this function starts from negative values at $\eta = 1$ and tends to zero as $\eta \to \infty$. The absolute value of G'(1) increases as Reynolds number increases.

Sample profiles of the real part of azimuthal component of velocity for pure harmonic motion of the cylinder for selected time variation ($\beta\tau$) are given in Figure 13, at Re = 1000 and S = 0. Here, the real azimuthal velocity component is shown for a complete period of oscillation.

Sample profiles of radial velocity are presented in Figure 14 for selected values of Reynolds number. As it is evident from this figure, because

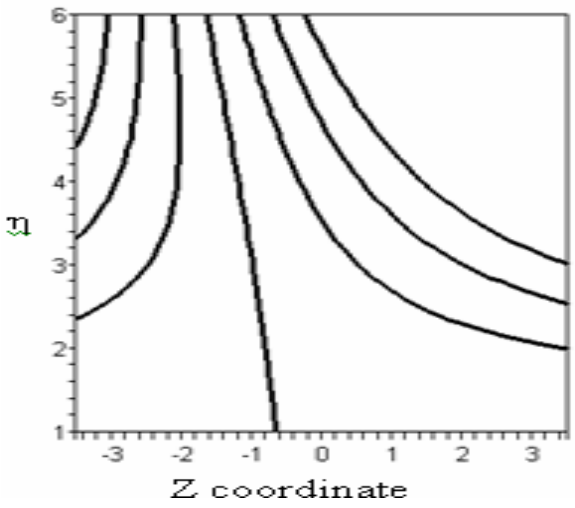

Figure 15. Streamlines in z–η plane for flow with S = 0, γ = 1 and Re = 1.

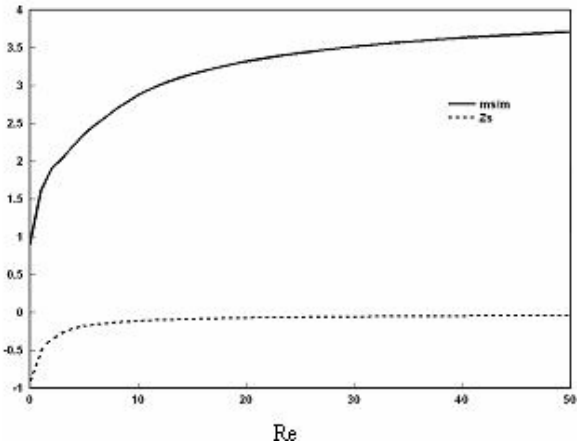

Figure 16. Variation of Z_s and m_s/m in terms of Reynolds number.

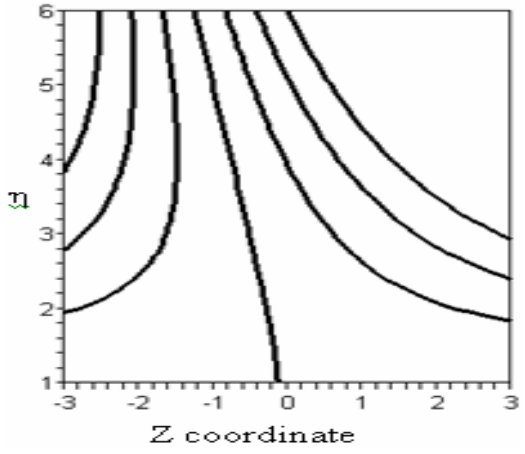

Figure 17. Streamlines in z–η plane for S = 0, γ = 1 and Re = 10.

of no transpiration the velocity is zero at η = 1 and after much increase inside the boundary layer increases with respect to η outside of this layer.

The flow streamlines in z–η plane are shown in Figures 15-18 for selected values of Reynolds number and γ. As it can be seen the intersection of $\Psi(\eta,z) = 0$ and the cylinder is not at z = 0, pointed out by Weidman [15]. Displacement of this point depends on the Reynolds number of the flow and increases as Re is smaller. In Figure 18 this displacement tends to zero because of the increase of flow momentum and decrease of boundary layer.

The real part of azimuthal shear stress component on the surface of the cylinder with harmonic rotation and with accelerating and decelerating oscillatory motions at Re = 1000 is presented in Figure 19, for transpiration rate S = 0. This shear - stress is for a complete period between 0 and 2π. It can be seen that as the frequency of the oscillation increases, the maximum of the absolute value of the shear - stress increases and β = 0 corresponds to the case of constant angular velocity in which the imaginary part of the azimuthal shear - stress is zero and its real part is a constant, as in Ref. [12]. Comparing Figures 13 and 19, it is concluded that the real part of azimuthal shear - stress and azimuthal velocity are in different phases. This figure also shows that the maximum of the absolute value of the real part of azimuthal shear - stress for $a > 0$ is more and for $a < 0$ is less than the case of pure oscillation. Also note that the phase - difference of shear - stress and azimuthal velocity decreases with increasing a.

Sample profiles of axial shear stress on the cylinder for selected values of Reynolds number and no transpiration are presented in Figure 20. As is clear from this figure, stress tensor increases linearly with Z and also increases as Renolds number increases.

Sample profiles of the θ(η) function for wall temperature and wall heat flux, both varying exponentially with time are presented in Figures 21 and 22, for selected values of Reynolds number, Prandtl number and transpiration rate. From 21, it is seen that as the rate of exponential function or suction rate increases, the depth of diffusion of the temperature field decreases and thus the heat

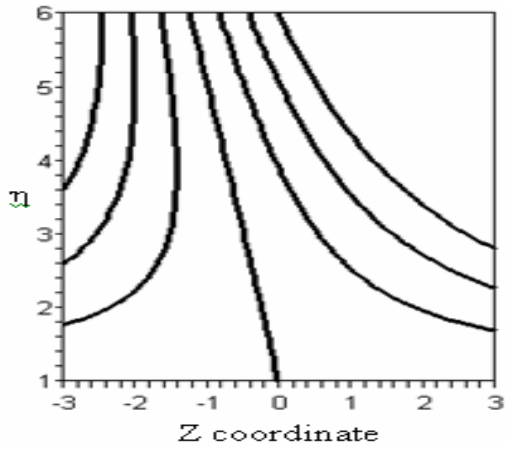

Figure 18. Streamlines in z–η plane for S = 0, γ = 1, at Re = 100.

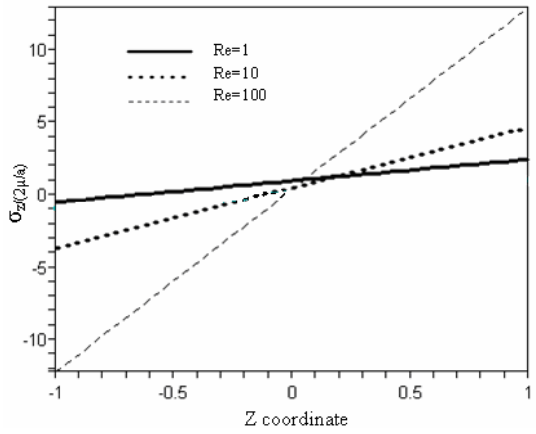

Figure 20. Variation of axial stress tensor on cylinder surface with respect to Reynolds number.

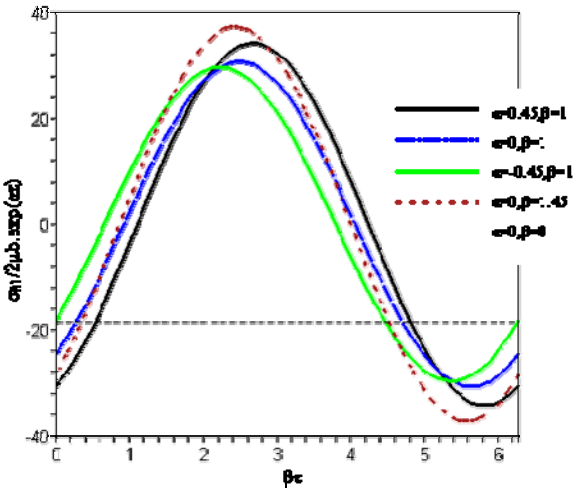

Figure 19. Real part of tangential stress tensor on the cylinder surface for different rotation situation and S = 0, at Re = 1000.

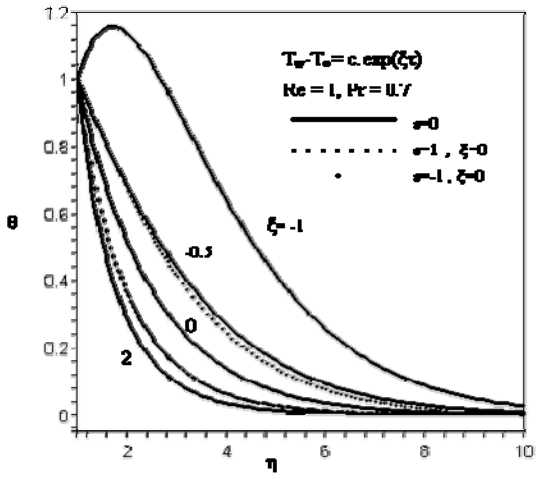

Figure 21. Temperature function with respect to η for known value of wall temp. for S = 0 and selected values of Re and Pr.

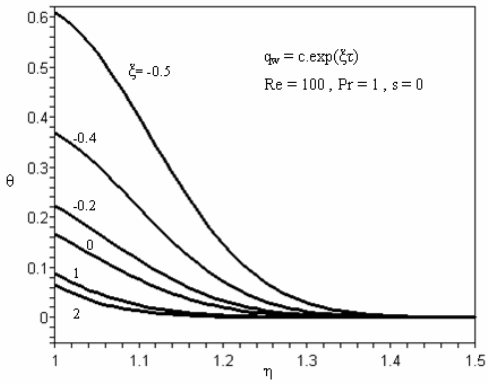

Figure 22. Temperature function with respect to η for known value of wall heat flux for S = 0 and selected values of Re and Pr.

transfer coefficient increases. From 22, it is noted that as the rate of exponential function increases, wall temperature and its depth of diffusion decreases. In Figure 21 for $\gamma < 0$, as the absolute value of γ increases, the fluid in the vicinity of the cylinder is not cooled as fast as the cylinder wall and therefore the fluid temperature here is greater than the wall temperature. It is interesting to note that for a particular negative value of γ, the slope of temperature on the surface is zero and therefore

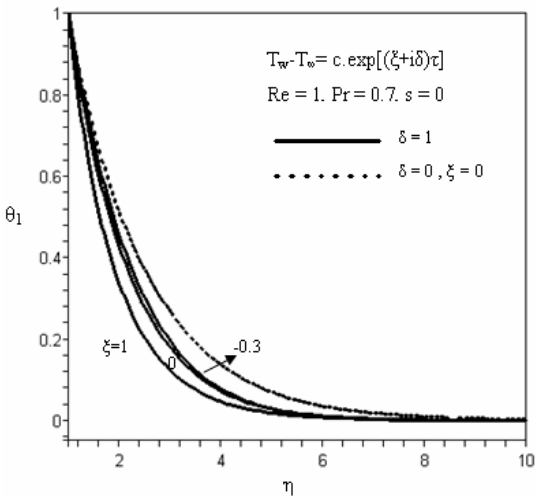

Figure 23. Temperature function with respect to η for known value of heat flux for S = 0 and selected values of Re and Pr.

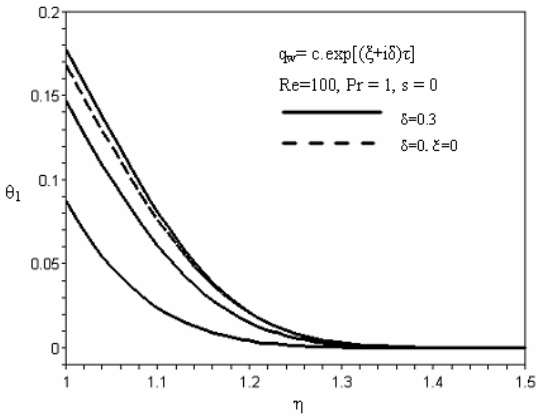

Figure 24. Temperature function with respect to η for known value of heat flux for S = 0 and selected values of Re and Pr.

there is no heat transfer. From both of these figures and γ = 0, the results of Ref. [9] are obtained.

Sample profiles of $\theta_1(\eta)$ function for wall temperature and wall heat flux, both varying with accelerating and decelerating oscillatory functions of time with different rates for transpiration rate S = 0 are given in Figures 23 and 24 for selected values of Reynolds number and Prandtl number. It is noted in Figure 23 that as the oscillation frequency increases, the initial slope of $\theta_1(\eta)$ increases. Further, as γ increases, the depth of the $\theta_1(\eta)$ decreases. From 24, as oscillation frequency increases, $\theta_1(\eta)$ and its depth of diffusion decrease. Also, as γ increases, the absolute value of $\theta_1(\eta)$ and its depth of diffusion decrease. From both of these figures and for δ = 0, the results of Ref. 9 are obtained.

Sample profiles of the $\theta_1(\eta)$ function for wall temperature and wall heat flux varying with an accelerating oscillatory function of time and for selected values of Prandtl number and Reynolds number are depicted in Figures 25 and 26, for transpiration rate S = 0. From 25, it is noted that as Prandtl number or Reynolds number increases, the depth of diffusion of the temperature field decreases rapidly and therefore the heat transfer coefficient increases. In 26, the absolute value of $\theta_1(\eta)$ function and its depth of diffusion decrease with increasing Prandtl number or Reynolds number.

Sample profiles of the real part of local heat transfer coefficient (Nusselt number) for (a) wall temperature and (b) wall heat flux varying with accelerating oscillatory functions for selected values of γ and δ in terms of Prandtl number at Re = 1000 are depicted in Figure 9 for S = 0. In both cases, Nusselt number increases as Prandtl number increases. Besides, as γ and δ increase, the real part of Nusselt number increases.

8. CONCLUSIONS

An exact solution of the Navier - Stokes equations and energy equation is obtained for the problem of stagnation - point flow obliquely impinging on a circular cylinder with uniform transpiration rate. The formulation of the problem, though, is for the more general case of time - dependent transpiration rate. A general self - similar solution is obtained when the cylinder has different forms of rotational motions including: constant angular velocity rotation, exponential angular velocity rotation, pure harmonic rotation, both accelerating and decelerating oscillatory rotations. Since the heat transfer is axisymmetric in the θ direction, the cylinder rotation has no effect on the temperature field. Results for different time-dependent wall temperature and heat flux functions including: constant wall temperature or heat flux, exponential and oscillatory form of wall temperature or wall

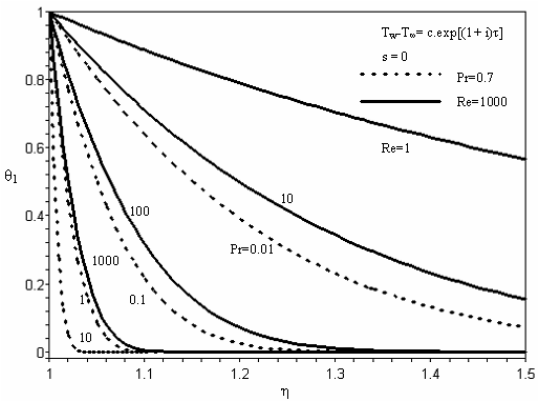

Figure 25. Temperature function with respect to η for known value of wall temp. for S = 0 and selected values of Re and Pr.

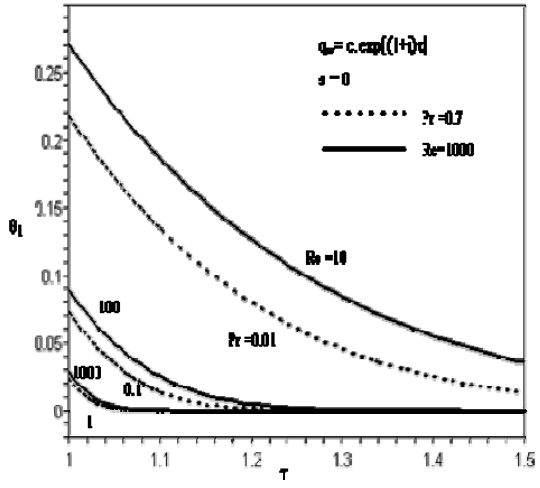

Figure 26. Temperature function with respect to η for known value of heat flux for S = 0 and selected values of Re and Pr.

heat flux are presented. Also, some sample semi - similar solutions for the same problem have been considered when the circular cylinder is rotating with different types of time - dependent angular velocity and also with time - dependent wall temperature or wall heat flux. The azimuthal component of fluid velocity and surface azimuthal shear - stress on the cylinder are obtained in all the above situations and for different values of Reynolds number and transpiration rates. The absolute value of the azimuthal shear - stress corresponding to all the cases increases with increasing Reynolds number and suction rate. Also, the maximum value of shear - stress increases with increasing oscillation frequency and accelerating and decelerating parameter *a* in the exponential amplitude function. In the defined wall temperature case, heat transfer increases with the increase of Reynolds number, Prandtl number and suction rate, whereas the depth of the diffusion of temperature field decreases. In the case of defined wall heat flux, the wall non - dimensional temperature, θ(η) and its depth of diffusion decrease with increase of Reynolds number, Prandtl number and suction rate. So, an increase of suction rate can be used as means of cooling the surface and increase of blowing can be used as means of heating the surface. It is shown that by providing blowing on the surface of a cylinder, a reduction of resistance against its rotation inside a fluid can be achieved. It is also shown that a cylinder spun up from rest in an exponential manner is azimuthaly stress - free for certain combinations of Reynolds number and rate of this exponential function. Further, it is found that higher suction rates are means for cooling the surface and higher blowing rates are means of heating the surface of the cylinder. An interesting result is also obtained showing that a cylinder with certain type of exponential wall temperature exposed to a temperature difference has no heat transfer. The local coefficient of heat transfer is found to be independent of time, though the temperature field is time - dependent.

9. NOMENCLATURE

a	Cylinder radius
b,c	Constant
f(η),f(η,τ)	Function
g(η),g(η,τ)	Function
h	Heat transfer coefficient
i	$\sqrt{-1}$
K	Thermal conductivity
m(η)	Function
m_s	Slope of the dividing streamline
N_u	Nusselt number
p	Pressure
Pr	Prandtl number
Q(τ)	Function

q_w	Wall heat flux
Re	Reynolds number
r,ϕ,z	Cylindrical coordinates
S	Dimensionless transpiration
t	Time
T	Temperature
T_w	Wall temperature
T_∞	Ambient temperature
u,v,w	Velocity components
U_o	Transpiration rate

Greek

α,β	Constants
$\overline{\alpha}$	Thermal diffusivity
Γ	Impinging stream strength
γ	Parameter
ξ,δ	Constants
η	Dimensionless radial variable
θ(η)	Function
Θ	Dimensionless temperature
μ	Fluid viscosity
ν	Kinematic viscosity
ρ	Density
σ	Shear stress
σ_ϕ	Azimuthal surface shear stress
τ	Dimensionless time
ϕ(η)	Function
Ψ(η,z)	Dimensionless streamfunction
ω	Angular velocity

10. REFERENCES

1. Wang, C., "Axisymmetric stagnation flow on a cylinder", ***Quarterly of Applied Mathematics***, Vol. 32, (1974), 207-213.
2. Stuart, J. T., "The viscous flow near a stagnation point when the external flow has uniform vorticity", ***J. Aero/Space Sci***., Vol. 26, (1959), 124-125.
3. Tamada, K., "Two - dimensional stagnation - point flow impinging obliquely on a plane wall", ***J. Phys. Soc. Japan***, Vol. 46, (1979), 310-311.
4. Dorrepaal, J. M., "An exact solution of the Navier - Stokes equation which describes non - orthogonal stagnation - point flow in two dimensions", ***J. Fluid Mech***., Vol. 163, (1986), 141-147.
5. Liu, T., "Nonorthogonal stagnation flow on the surface of a quiescent fluid - an exact solution of the Navier - Stokes equation", ***Quart. Appl. Math.***, Vol. 50, (1992), 39-47.
6. Tilley, B. S. and Weidman, P. D., "Oblique two - fluid stagnation - point flow", ***Eur. J. Mech. B/ Fluids***, Vol. 17, (1998), 205-217.
7. Gorla, R. S. R., "Transient response behavior of an axisymmetric stagnation flow on a circular cylinder due to a time dependent free stream velocity", ***Lett. Appl. Eng. Sci***., Vol. 16, (1978), 493-502.
8. Gorla, R. S. R., "Unsteady viscous flow in the vicinity of an axisymmetric stagnation - point on a cylinder", ***Int. J. Engineering Science***, Vol, 17, (1979), 87-93.
9. Gorla, R. S. R., "Heat transfer in an axisymmetric stagnation flow on a cylinder", ***Applied Scientific Research J***., Vol. 32, (November 1976), 541-553.
10. Cunning, G. M., Davis, A. M. J. and Weidman, P. D., "Radial stagnation flow on a rotating cylinder with uniform transpiration", ***Journal of Engineering Mathematics***, Vol. 33, (1998), 113-128.
11. Rahimi, A. B., "Heat transfer in an axisymmetric stagnation flow on a cylinder at high Prandtl numbers using perturbation techniques", ***Int. J. of Engr. Science***, Vol. 10, No. 3, (1999).
12. Saleh, R. and Rahimi, A. B., "Axisymmetric stagnation - point flow and heat transfer of a viscous fluid on a moving cylinder with time - dependent axial velocity and uniform transpiration", ***Journal of Fluids Engineering***, Vol. 126, (November 2004).
13. Peregrine, D. H., "The fascination of fluid mechanics, ***J. Fluid Mech***., Vol. 106, (1981), 59-80.
14. Hiemenz, K., "Die Grenzchicht an einem in den gleichformingen flussigkeitsstrom eingetauchten geraden kreiszylinder", ***Dinglers Polytech. J***., Vol. 326, (1911), 321-410.
15. Weidman, P. D. and Putkaradze, V., "Axisymmetric stagnation flow obliquely impinging on a circular cylinder", ***European J. of Mechanics B/Fluids***, Vol. 22, (2003), 123-131.
16. Press, W. H., Flannery, B. P., Teukolsky, S. A. and Vetterling, W. T., "Numerical recipes, the art of scientific computing", Cambridge University Press, Cambridge, (1997).